







Wireless Powered Dielectric Elastomer Actuator

Lai Chen , Takuya Sasatani , Keung Or, Satoshi Nishikawa , Yoshihiro Kawahara ,
Ryuma Niiyama , and Yasuo Kuniyoshi 

Abstract—The need for cable connection with soft robotic systems suppresses the benefits granted by their softness and flexibility. Such systems can be untethered by equipping batteries or by relying on non-electrical actuation mechanisms. However, these approaches cannot simultaneously support long-term and intelligent operations. This research examines a proposed wireless soft actuator based on wireless power transfer (WPT) and dielectric elastomer actuator (DEA) technology, thereby realizing soft robot more diversified application and long-term locomotion. A compact conical DEA fabrication process is presented with 6 mm periodic linear output and design of a lightweight WPT receiver that weighs only 13 g integrated with a driver circuit. Evaluation results show that this system remotely powers the DEA and the intelligent peripheral circuits for system control. Furthermore, our design seamlessly bridges the WPT system, power-efficient in low-voltage output conditions, and the DEA, which requires high-voltage input (kV) for deformation, by leveraging high-voltage boost-converters. Experimentally obtained results demonstrate untethered DEA operation at 170 mm from the transmitter. Also, we demonstrated applying this DEA as a wireless pump.

Index Terms—Soft robotics, Wireless power transmission..

I. INTRODUCTION

SOFT robotics technology can adopt the softness and flexibility of soft materials to help robots adapt to various unstructured environments. For soft robotic systems, cable connections are often necessary to transmit energy from power resources to the robot. Untethered systems can liberate the robots, but traditional systems often rely on bulky on-board components such as batteries and pumps [1]. These power resources make robots heavy and limit their operation time. Therefore, large-capacity components are needed for long-term operation, which is unsuitable for small-scale robots. Some recent works have used non-electrical actuation power resources such as light [2] and magnetic fields [3]. Although these new approaches can enable soft robots to work flexibly, compatibility is a problem

Manuscript received February 24, 2021; accepted June 22, 2021. Date of publication July 14, 2021; date of current version July 29, 2021. This letter was recommended for publication by Associate Editor J. Rossiter and Editor C. Laschi upon evaluation of the reviewers' comments. This work was supported by JST ERATO under Grant JPMJER1501 and in part by JSPS KAKENHI under Grants JP18H05466 and JP20K19890. (Corresponding author: Lai Chen.)

Lai Chen, Keung Or, Satoshi Nishikawa, Ryuma Niiyama, and Yasuo Kuniyoshi are with the Graduate School of Information Science and Technology, The University of Tokyo, Tokyo, Japan (e-mail: chenlai@isi.imi.i.u-tokyo.ac.jp; or@isi.imi.i.u-tokyo.ac.jp; nisikawa@isi.imi.i.u-tokyo.ac.jp; niiyama@isi.imi.i.u-tokyo.ac.jp; kuniyosh@isi.imi.i.u-tokyo.ac.jp).

Takuya Sasatani and Yoshihiro Kawahara are with the Graduate School of Engineering, The University of Tokyo, Tokyo 113-8654, Japan (e-mail: sasatani@akg.t.u-tokyo.ac.jp; kawahara@akg.t.u-tokyo.ac.jp).

Digital Object Identifier 10.1109/LRA.2021.3097271

for power resources of these kinds and the common peripheral elements such as sensors and microcontrollers in the robot.

Wireless power transfer (WPT) technology promises to empower both power-hungry actuators and intelligent electrical components remotely. By offloading the power supply function to an external power transmitter, robots equipped with power receivers can operate over a long periods without integrating power wires or bulky batteries. Among the various WPT approaches, we leverage the magnetic resonance coupling approach introduced by MIT in 2007 [4]: (i) It can transmit great amounts of power over mid-range distances. (ii) It is robust to misalignment and can be deployed on soft robots in various form factors. (iii) It can operate in various media (*e.g.*, underwater). In general, components inside robots such as sensors and actuators are powered by electricity. The use of conventional untethered power transmission methods such as light requires additional energy conversion for converting electricity in other forms and often causes large energy loss through transformation. Different from traditional batteries, robots based on WPT have long operation time with the support of external transmitters. Furthermore, the receiver coil on the robot, as a power resource, is light and designable. Consequently, it can well fit with the robot structure and make robots more compact.

An electrical soft actuator is a reasonable choice for cooperation with WPT because it does not need the complicated energy conversion which causes marked energy loss. Common electrical soft actuators mainly include shape memory alloy (SMA), ionic polymer-metal composite (IPMC), and dielectric elastomer actuator (DEA). The work of SMA is based on thermoelastic martensites transformation. It can function with low voltage, but it requires high current for actuation which often leads to large power consumption. The work of IPMC is based on relocation of ion in the polymer. Although it can generate a large stroke with low voltage, the response is extremely slow: one stroke can take up to 3.5 s. The output stress and efficiency are low [5]. Furthermore, it must function in high-moisture environments. Moreover, IPMC fabrication is environmentally unfriendly and too complicated to be realized because of the usage of fluorinated polymers and noble metallic electrodes through a complex and time-consuming electro-less plating process [6]. The work of DEA is based on the Maxwell stress produced by the flexible electrodes on the DE membrane. It is presumably of light weight, low energy cost, large strain, and fast response. Consequently, it is more suitable than SMA and IPMC for the development of flexible soft robots as long as high DC voltage is applicable to it with smaller and lighter power resources.

Jumping robots [7] and crawling robots [8] based on WPT and SMA and swimming robots [9] based on WPT and IPMC have been developed. However, robots equipped with WPT and DEA have not been reported. Therefore, the use of WPT to improve the independence of DEA is challenging. Specifically, DEA works in high-voltage (kV) DC, whereas WPT works in low-voltage (V) and high-frequency AC. Few reports have described WPT supporting such a large voltage boost. Among all kinds of DEA, a conical configuration has been widely adopted for soft actuation applications including a multiple degrees-of-freedom (DOF) platform [10], a crawling robot [11], and a flapping robot [12]. Because, to provide new solutions for realizing more flexible untethered soft robots, we proposed a wirelessly powered conical DEA with great application potential in this work.

Detailed challenges of this work include the fabrication of DEA with large stroke and an adjustable period, establishment of an effective on-board wireless power supply and realization of a circuit that matches the electricity of WPT and DEA. The exposition in this letter is arranged in five sections. Chapter II describes the DEA design and fabrication process and analyzes its characterization by theory and experimentation. Chapter III introduces the WPT system. Chapter IV presents the conversion circuit connecting WPT and DEA. Chapter V presents the performance of whole-system integration with an application to a pump. Finally, Chapter VI concludes our work and presents prospects based on the work and findings described herein.

II. CONICAL DIELECTRIC ELASTOMER ACTUATOR

A. Design

DEA can be designed into various configurations for generating outputs of various kinds such as linear, bending, and rotation. The conical configuration has been used widely because of its great compactness, ease of fabrication, and large actuation stroke. Conical DEA is divisible into three configurations including linear compression spring, biasing mass, and antagonistic double-cone DEA according to the bias. Among these three configurations, double-cone configuration has largest stroke, single-cone with biasing mass has the greatest output stress, linear spring configuration is the most compact. In consideration of the system size, DEA with linear compression spring is designed in current work because of its compact structure. The mathematical model of this DEA proposed by He *et al.* [13] is readily available in the literature. DEA consists of a piece of DE membrane with flexible electrodes on two sides. As Fig. 1 shows, the membrane is adhered to a circular acrylic holding frame and is fixed to a basement with biasing mechanism and linear spring. The biasing mechanism produces protrusion force and pushes the membrane out of plane to form a conical geometry and provide DEA with pre-stress. To avoid concentration of stress at the place where the mechanism contacts with the membrane, the edge of mechanism has been chamfered. When high voltage is applied to DEA, the Maxwell stress generated by electrodes will extrude DEA and release the pre-stress to provide output. The guide in the center of basement is designed to ensure the linear output.

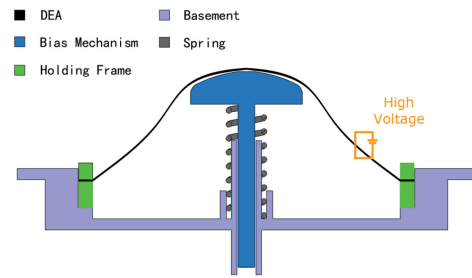


Fig. 1. Cross-section view of the conical DEA.

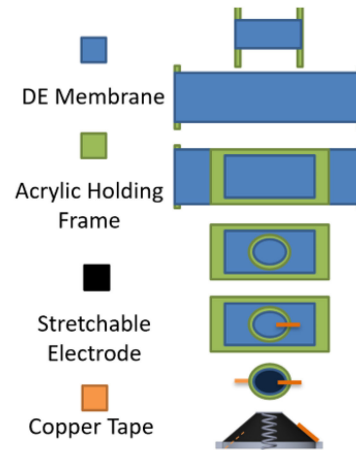


Fig. 2. Fabrication process of conical DEA.

B. Fabrication

We used a 3D printer (ProJet MJP 2500; 3D Systems, Inc., USA) to fabricate the basement and biasing mechanism. Then we installed the biasing mechanism with linear spring to the basement. Fig. 2 presents the fabrication of DEA divided into seven steps: (1) cut a piece of DE membrane (VHB Y4910 J; 3M, USA) with suitable size; (2) biaxially stretch the membrane at the ratio of 2.5; (3) clamp the membrane by acrylic holding frame to maintain the stretch state; (4) adhere the acrylic rings to both sides of membrane with silicone adhesive (Sil-Poxy; Smooth-On, Inc., USA); (5) stick the copper tape to both sides of membrane; (6) apply carbon grease (Carbon Grease; Kitaco Co., Ltd., Japan) evenly to both sides of membrane; (7) cut out the DEA and install it to the basement.

C. Characterization

Two experiments were conducted, as described in this section, to analyze the conical DEA characteristics. Displacement measurement experiment based on motion capture and force measurement experiment based on force gauge. Although the pre-stretch we adopted is helpful for avoiding electric breakdown, the long-term continuous work still causes electric breakdown [14]. The DE needs time to reach to the desired position in these two power states because of its viscoelasticity. Consequently, after weighing the effectivity and safety, 333 mHz was selected as the frequency; the duty is 40%. The periodic signal from the arbitrary function generator (FGX-2220; Texio

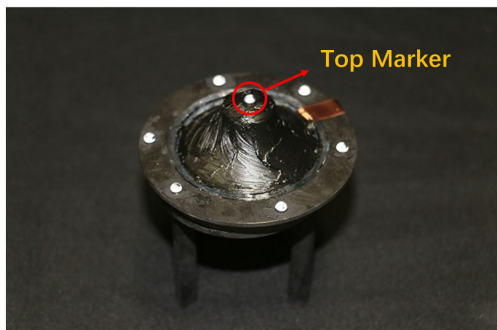


Fig. 3. Conical DEA for displacement experiment.

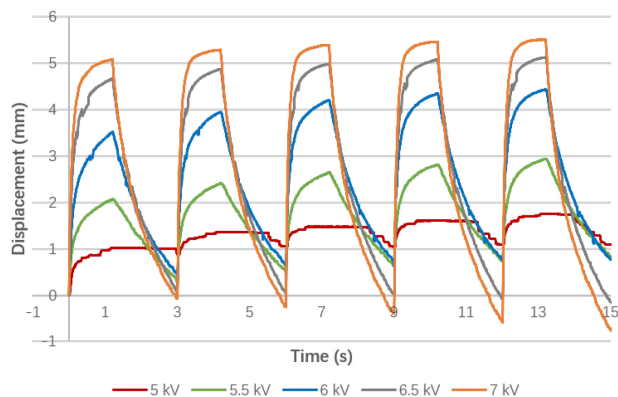


Fig. 4. Results of displacement measurement experiments.

Technology Corp., Japan) goes through the power amplifier (HSA4101; NF Corp., Japan) and boost converter for separate generation of the periodic output of 5 kV, 5.5 kV, 6 kV, 6.5 kV, and 7 kV for actuation of DEA. Because the displacement change and force change between 5 kV and 7 kV are not large, we determined the interval of the change of input voltage to be 0.5 kV. The deformation of DEA will be too small to be appreciated if the voltage is lower than 5 kV. Voltage higher than 7 kV can be expected to cause electric breakdown.

For the displacement experiment, we placed six markers around the conical DEA to mark the basement and one marker on the top of the DEA for displacement sampling (Fig. 3). A motion capture system (OptiTrack; NaturalPoint, Inc., USA) and four cameras (Flex 13; NaturalPoint, Inc., USA) were used for obtaining marker positions. The position of the top marker was recorded. The displacement is defined as the position change of this marker in a vertical direction from the beginning. The result is portrayed in Fig. 4. The difference of displacement between peak and bottom is defined as the stroke. The average strokes with standard deviations are presented in Fig. 5. When the input within the range of 5 kV and 7 kV, the DEA can function effectively and stably. Furthermore, according to the fitted trend curve, with the increase of voltage, the stroke of DEA increases gradually. The maximum average stroke in the stable working state can be up to around 6 mm when the input is 7 kV.

To measure the contact force during experimentation, we used a force gauge (FGP-1; Nidec Corp., Japan) and a test stand (FGS250VC; Nidec Corp., Japan). The experiment setup

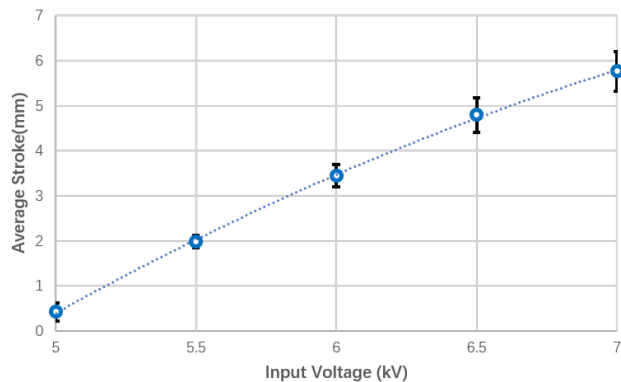


Fig. 5. Average stroke with standard deviations and fitted curve.

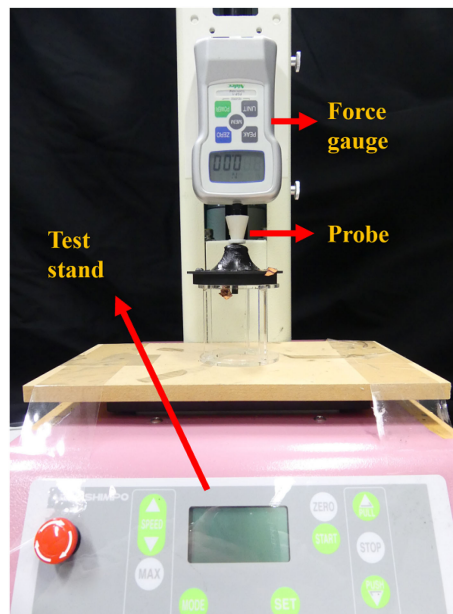


Fig. 6. Experiment setup for contact force measurement.

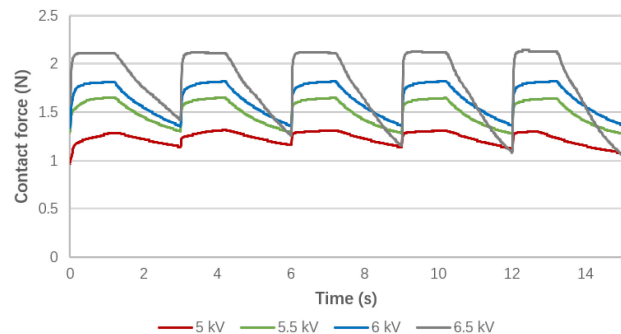


Fig. 7. Results of contact force measurement experiments.

is depicted in Fig. 6. In the initial state, the DEA was mounted to the test stand with the condition that the probe of force gauge just contacts with the surface of the top of DEA. Subsequently, 5-6.5 kV inputs were exerted to DEA. The corresponding contact force from the force gauge was recorded results are shown in Fig. 7. The difference of contact force between the peak

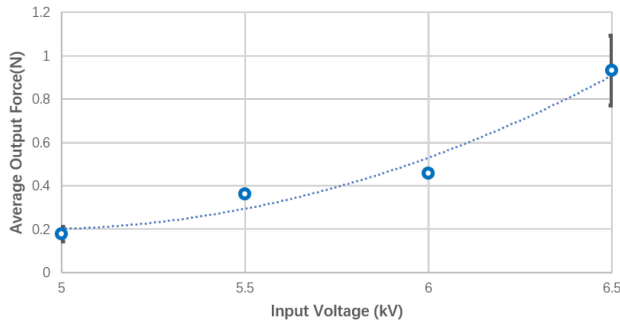


Fig. 8. Average output force with standard deviations and fitted curves.

and bottom is defined as the output force. The average output forces are shown with standard deviations in Fig. 8. According to the fitted trend curve, the output force of DEA increases gradually with the increase of voltage. The maximum output force is approximately 0.9 N. Regarding the 7 kV input, when the DE membrane exerted pushing force against the force gauge, with the situation that Maxwell stress gives the DE membrane a rather thinner condition: the DEA became unstable and caused an electrical breakdown. Therefore, the 7 kV result is missing from Fig. 7.

The common aspect of the two experiments above is that there is hysteresis for DEA recovery when the input voltage is low. Furthermore, DEA cannot recover to initial state immediately without the help of external force. This phenomenon is attributable to factors including the material's viscoelasticity, residual charge, and friction between the bias mechanism and DEA.

III. WIRELESS POWER TRANSFER

Many physical phenomena support WPT technologies, including light propagation [15], electromagnetic induction [16], electrical field (*i.e.*, displacement current), microwaves [17], and acoustic waves [18]. For this study, the magnetic resonance coupling approach introduced by MIT in 2007 is leveraged, which transfers power between a pair of inductively coupled high-Q LC resonators [4]. This approach enables supply of high-power levels at midrange distances; it is robust to positional misalignment [16], [19]. In addition to these general advantages, this approach offers the following benefits, which makes it promising for empowering soft robots: (i) it enables power supply in various media (*e.g.*, underwater); (ii) its high frequency operation enables light receiver coils; and (iii) we can adjust the lumped capacitors' values to compensate for coil form-factor changes, enabling receiver shapes that are amenable to application in soft robots.

When abstracted to a circuit model, our system involves a pair of inductively coupled coils terminated with capacitors that tune each coil's resonant frequency. Fig. 10 portrays the equivalent circuit of the studied system: L_{TX} , L_{RX} , C_{TX} , C_{RX} , R_{TX} , and R_{RX} respectively denote the inductance, capacitance, and the copper loss of the transmitter (TX) and receiver (RX), whereas M represents the mutual inductance between the transmitter and receiver coil. R_{load} is the equivalent impedance of the

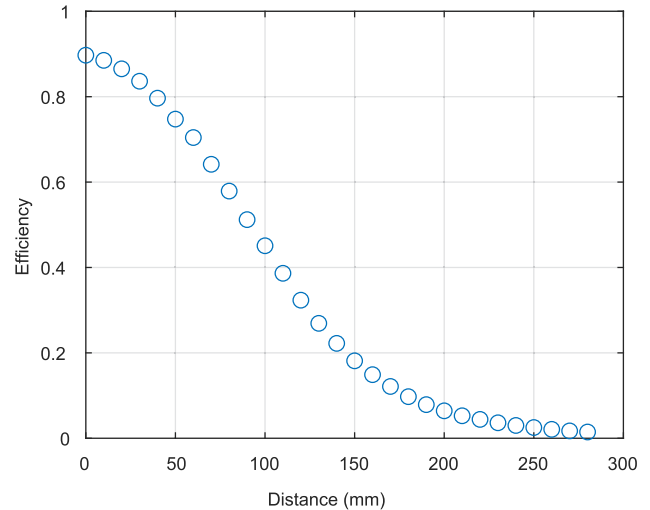


Fig. 9. Power transfer efficiency with varying distance.

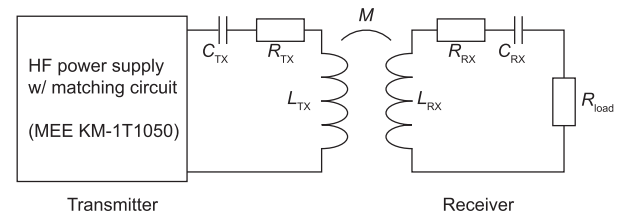


Fig. 10. System diagram for wireless power transfer.

TABLE I
PARAMETERS OF TX AND RX COILS

Parameters	TX Coil	RX Coil
Diameter of Coil [mm]	136	54
Wire diameter [mm]	2.0	0.5
Number of turns	6	12
Inductance L	11.0 μ H	14.7 μ H
Quality Factor (Q)	196	110

actuator circuit. Consequently, the goal of this system is to push power into this equivalent load. Table. I presents the geometric parameters of the coil and the resulting electronic properties. We determined the capacitor values based on the measured inductance values using the following series resonance condition [19].

$$2\pi f_0 = \frac{1}{\sqrt{LC}} \quad (1)$$

In that equation, f_0 represents the resonant frequency of the coils. We set this resonant frequency to 6.78 MHz, which is often used in WPT applications because it is an industrial scientific and medical (ISM) band. In this frequency band, the WPT system safety is evaluated based on the specific absorption rate (SAR) (*i.e.*, the energy absorbed by tissue per weight). Earlier work has demonstrated that the magnetic resonance coupling technique can deliver high power more safely than other methods such as microwaves and lasers [20].

Next, we proceed with evaluation of the power transfer efficiency between the transmitter and receiver coils when we vary

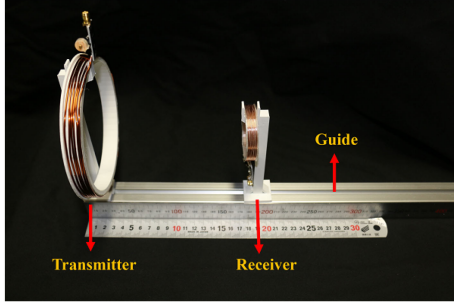


Fig. 11. Setup for evaluating power transfer efficiency between the transmitter and receiver coils.

the distance separating the coils. Fig. 11 shows the evaluation setup with the transmitter and receiver coils. We performed two port measurements using a vector network analyzer for obtaining the S-parameter matrix (*i.e.*, scattering matrix). We processed these parameters to evaluate the power transfer efficiency. We calculated efficiency η_{\max} using the following formula, which corresponds to the maximum power transfer efficiency of a given two-port network [21], [22].

$$\eta_{\max} = \frac{\chi}{(1 + \sqrt{1 + \chi})^2} \quad (2)$$

$$\chi = \frac{|Z_{12}|^2}{rZ_{11}rZ_{22} - rZ_{12}^2} \quad (3)$$

Here, $rZ = \text{re}\{Z\}$ and $iZ = \text{im}\{Z\}$. Z is the Z -parameter matrix, converted from the measured S-parameter matrix. The power transfer efficiency of WPT systems generally depends on the load impedance R_{load} . Also, (2) represents the efficiency attained when tuning the load impedance to match the value which maximizes efficiency, giving insight into the coupled coils' fundamental characteristics.

Fig. 9 presents the efficiency measured through the procedure described above. Decay in transfer efficiency with increasing distance can be observed. The efficiency is about 6% at a 200 mm distance. Because the minimum power consumption of the studied actuator is about 0.6 W, this result indicates that the studied actuator can be operated at 200 mm distances with 10 W input. The maximum transmission power of the transmitter is 12 W. Therefore, the effective operation distance is 200 mm or more.

IV. CONVERSION CIRCUIT

Next, we discuss the design of the conversion circuit which bridges WPT and the DEA. The WPT receiver outputs high-frequency (MHz) power. The DEA requires high voltage (kV) DC for actuation. Actually, DEA can be treated as a capacitive load with small power consumption (10^{-3} W) [23], which requires high voltage and small current, leading to high impedance loading conditions. However, series resonant WPT systems tend to suffer from the decrease in efficiency when directly supplying power to high impedance loads in loosely coupled conditions [24], which our system typically experiences. To

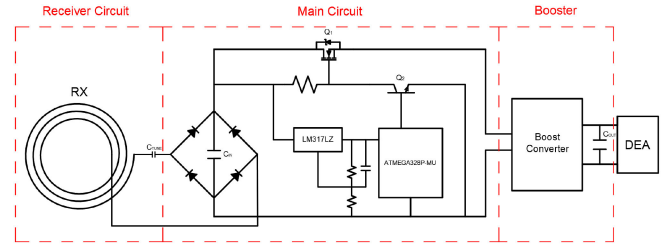


Fig. 12. Actuator circuit schematic.

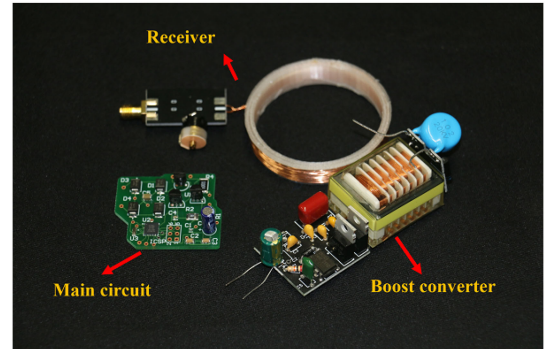


Fig. 13. Elements of the actuator circuit.

bridge WPT and DEA, we design a conversion circuit with the receiver, rectifier, periodic DC voltage generator, and an HV boost converter. This circuit appropriately boosts the output voltage and lowers the equivalent load impedance (*i.e.*, voltage/current ratio) for moving into operating ranges where efficient WPT is achievable.

Fig. 12 is the onboard circuit schematic for wirelessly powered DEA. To reduce the total size and weight, the main circuit was designed to be as compact as possible. The transmitter delivers power to the main circuit via the receiver. When the receiver's position or the output of the power source changes, the receiver output changes. Therefore, we designed the main circuit to be compatible with high-frequency input between 9 V and 30 V. A full-bridge rectifier consisting of four fast recovery diodes (MURS120T3G; ON Semiconductor, Semiconductor Components Industries LLC, USA) and filter capacitor C_{IN} converts the AC inputs to DC voltage. This power input powers both the control circuit and the boost converter used for driving the DEA. The control circuit includes a linear voltage regulator and a microcontroller (ATMEGA328P-MU; Microchip Technology Inc., USA). This control circuit generates a periodic control signal that determines whether the circuit supplies power to the latter high-voltage boost converter via the high-side switch composed of MOSFET Q_1 and Transistor Q_2 . In this way, we can control the working period and duty cycle of DEA indirectly. The boost converter (DP-NC; Henan Guangao Electronics, China) we used can boost the voltage from 9.2-30 V to 2-20 kV. It can also be replaced by other common boost converters (e.g. EMCO Q101-5; XP Power, Singapore) for DEA. Fig. 13 shows the separated actuator circuit including receiver, main circuit, and boost converter. We fabricated the main circuit using 39 mm \times 37 mm \times 1.6 mm printed circuit boards (PCBs)

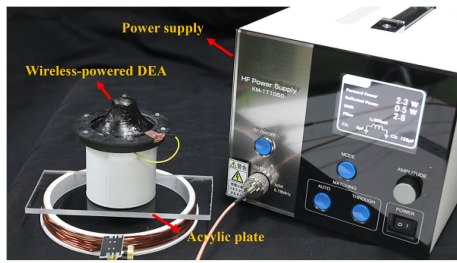


Fig. 14. Fully assembled wireless powered DEA.

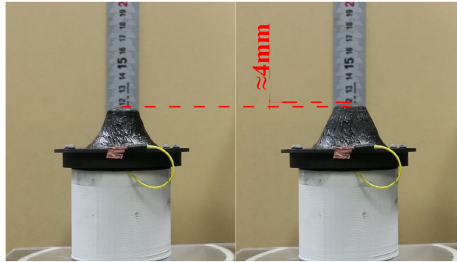


Fig. 15. Comparison between low voltage state (the left) and high voltage state (the right) when the actuator is in a working state.

with two layers. we evaluated the output power by replacing the boost converter with a 120 Ohm load and observing the input voltage. From comparison of the output power and input power, we estimated the energy efficiency of the main circuit (as shown in Fig. 12 and Fig. 13) as about 25%.

V. EXPERIMENT

A. Integration

Fig. 14 portrays a working fully assembled wireless powered DEA. Its total weight is 130 g, including a 13 g receiver coil, a 5 g control circuit, and a 50 g DC-DC converter. All parts were integrated into a cylindrical container (30 mm radius, 50 mm height) to produce a unit that can actuate DEAs of various sizes. The radius of DEA we used here is 26 mm. We set the actuator to work at 333 mHz with a duty cycle of 40% when receiving a sufficient amount of power. This actuator can work at input of 0.6-2 W. As a preliminary demonstration of wireless power transmission, we separated the actuator from the transmitter with some stacked transparent acrylic plates, each with 5 mm thickness. Fig. 15 shows the actuator's working state at low voltage (0 V) and high voltage (6.2 kV) when the input power is 1.5 W. The attachment video demonstrates the effect of the actuator both when the transmitter inputs low power and high power. We changed the acrylic plates' stacked numbers to vary the distance between the actuator and the transmitter. In this way, we demonstrated the relation between the actuator's maximum working distance and the input power. As presented in Fig. 16, the maximum working distance of the actuator is 170 mm. We observed that the increase rate of working distance decreases gradually with the increase of input power. This finding is consistent with the change pattern of transmission efficiency with distance revealed in Fig. 9.

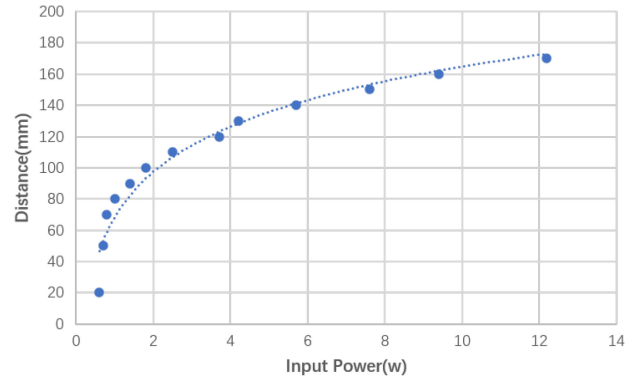


Fig. 16. Relation between input power and transfer distance.

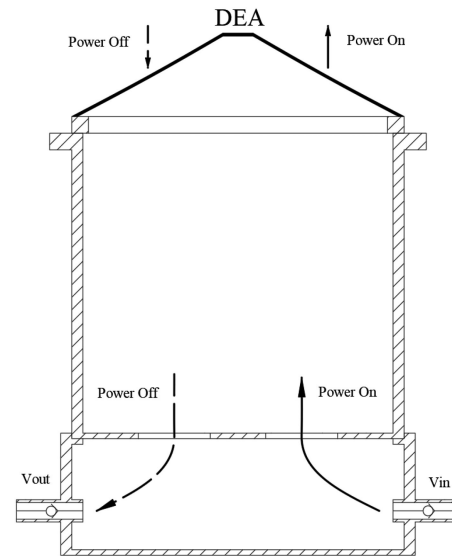


Fig. 17. Schematic image of the pump.

B. Pump Based on Wireless Powered DEA

To demonstrate the wireless powered DEA with a load further, we designed a pump based on the proposed wireless powered DEA. As Fig. 17 shows, this pump consists of sealed wireless powered DEA and two low cracking pressure check valves (V_{in} , V_{out} in Fig. 17; CVLU44; Nihon Pisco Co., Ltd., Japan). When the DEA was powered on, the DEA deformation increased the inner volume of the pump and led to the decrease of air pressure inside the pump. The decrease of inner pressure makes V_{in} open and V_{out} closed. Consequently, the pump intakes fluid through V_{in} . By contrast, if we power off the DEA, DEA recovers to its initial state and the inner volume of pump will be reduced. The increase of inner pressure closes V_{in} and opens V_{out} . It allows the pump to discharge the fluid through V_{out} . The pumping function can be realized by continuously alternating the power state of DEA. A demonstration showing the flow of pump is presented in the attached video. Fig. 18 shows the setup of the pumping experiment. In the experiment, the pump was placed at the center of the transmitter to ensure the maximum transfer efficiency of WPT. The valves and pump were connected by a silicone tube with 4 mm outer diameter and 3 mm inner

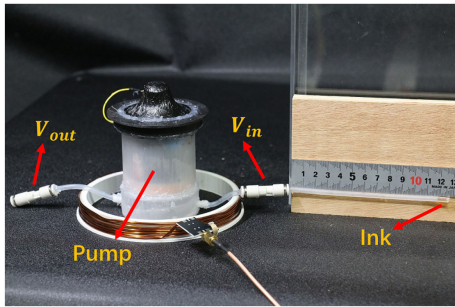


Fig. 18. Pumping test.

diameter. Another tube of the same size was connected to the inlet of V_{in} . The tube orientation was kept horizontal during the experiment. We injected 0.1 ml ink to this tube to evaluate the flow. When the input power of the whole system was set to 2 W, the DEA stroke on the pump was 2 mm less than that of DEA with no load. In a stable working state, each work cycle flow is 0.7-1.5 ml. Distribution occurred because of imperfect sealing. This pump can be greatly anticipated for application to artificial organs for transporting blood throughout the body or other gentle pumping system. There are three reasons: (i) Compared with hydraulic and pneumatic systems, its structure is more compact. (ii) The muscle-like material and mild transport mode can avoid damage to blood caused by the motor shear force [25]. (iii) Characteristics of wireless, low energy cost, and mutability make the application promising. Future work will investigate details of wireless DEA applications. Quantitative analysis of aspects such as efficiency will also be conducted.

VI. CONCLUSION AND DISCUSSION

This report is the first of an untethered DEA, remotely empowered via WPT technology. Experiments verified that our proposed on-board WPT system can provide sufficient power for conical DEA. The operating range can reach 170 mm distance from the transmitter. This advancement will liberate DEA from restrictions of cables and preserve the benefits granted by soft actuators' softness and flexibility. One direction of future work is to reduce the DEA size and optimize the WPT-DEA system performance. Beyond these improvements, our system can be applied to various small, lightweight, soft robotics systems to realize implantation of medical applications such as the pump we demonstrated or robot locomotion such as walking and swimming.

REFERENCES

[1] S. Rich, R. Wood, and C. Majidi, "Untethered soft robotics," *Nature Electron.*, vol. 1, no. 2, pp. 102–112, 2018.
 [2] C. Ahn, X. Liang, and S. Cai, "Bioinspired design of light-powered crawling, squeezing, and jumping untethered soft robot," *Adv. Mater. Technol.*, vol. 4, no. 7, 2019, Art. no. 1900185.

[3] Z. Ren, W. Hu, X. Dong, and M. Sitti, "Multi-functional soft-bodied jellyfish-like swimming," *Nature Commun.*, vol. 10, no. 1, pp. 1–12, 2019.
 [4] A. Kurs, A. Karalis, R. Moffatt, J. Joannopoulos, P. Fisher, and M. Soljačić, "Wireless power transfer via strongly coupled magnetic resonances," *Science*, vol. 317, no. 5834, pp. 83–86, 2007.
 [5] J. Shintake, "Functional soft robotic actuators based on dielectric elastomers," PhD thesis, EPFL, 2016.
 [6] J. Kim, J. W. Kim, H. C. Kim, L. Zhai, H. Ko, and R. M. Muthoka, "Review of soft actuator materials," *Int. J. Precis. Eng. Manuf.*, vol. 20, no. 12, pp. 2221–2241, 2019.
 [7] R. Kurniawan *et al.*, "An untethered 216-mg insect-sized jumping robot with wireless power transmission," in *Proc. IEEE/RSJ Int. Conf. Intell. Robots Syst.*, 2020, pp. 7881–7886.
 [8] C. McCaffrey *et al.*, "Continuum robotic caterpillar with wirelessly powered shape memory alloy actuators," *Soft Robot.*, vol. 7, no. 6, pp. 700–710, 2020.
 [9] K. Abdelnour, M. Stinchcombe, A. Porfiri, S. Zhang, and J. Childress, "Wireless powering of ionic polymer metal composites toward hovering microswimmers," *IEEE/ASME Trans. Mechatronics*, vol. 17, no. 5, pp. 924–935, 2011.
 [10] A. Conn and J. Rossiter, "Towards holonomic electro-elastomer actuators with six degrees of freedom," *Smart Mater. Structures*, vol. 21, no. 3, 2012, Art. no. 0 35012.
 [11] C. Nguyen *et al.*, "Printable monolithic hexapod robot driven by soft actuator," in *Proc. IEEE Int. Conf. Robot. Automat.*, 2015, pp. 4484–4489.
 [12] C. Cao, S. Burgess, and A. T. Conn, "Toward a dielectric elastomer resonator driven flapping wing micro airvehicle," *Front. Robot. AI*, vol. 5, p. 137, 2019.
 [13] T. He, L. Cui, C. Chen, and Z. Suo, "Nonlinear deformation analysis of a dielectric elastomer membrane-spring system," *Smart Mater. Structures*, vol. 19, no. 8, 2010, Art. no. 0 85017.
 [14] J.-S. Plante and S. Dubowsky, "Large-scale failure modes of dielectric elastomer actuators," *Int. J. Solids Structures*, vol. 43, no. 25/26, pp. 7727–7751, 2006.
 [15] V. Iyer, E. Bayati, R. Nandakumar, A. Majumdar, and S. Gollakota, "Charging a smartphone across a room using lasers," in *Proc. ACM Interactive, Mobile, Wearable Ubiquitous Technol.*, vol. 1, no. 4, pp. 1–21, 2018.
 [16] S. Y. R. Hui, W. Zhong, and C. Lee, "A critical review of recent progress in mid-range wireless power transfer," *IEEE Trans. Power Electron.*, vol. 29, no. 9, pp. 4500–4511, Sep. 2014.
 [17] N. Shinohara, "Power without wires," *IEEE Microw. Mag.*, vol. 12, no. 7, pp. S 64–S73, Dec. 2011.
 [18] H. Basaeri, D. B. Christensen, and S. Roundy, "A review of acoustic power transfer for bio-medical implants," *Smart Mater. Structures*, vol. 25, no. 12, 2016, Art. no. 123001.
 [19] A. P. Sample, D. T. Meyer, and J. R. Smith, "Analysis, experimental results, and range adaptation of magnetically coupled resonators for wireless power transfer," *IEEE Trans. Ind. Electron.*, vol. 58, no. 2, pp. 544–554, Feb. 2011.
 [20] J. Garnica, R. Chinga, and J. Lin, "Wireless power transmission: From far field to near field," *Proc. IEEE Proc. IRE*, vol. 101, no. 6, pp. 1321–1331, Jun. 2013.
 [21] M. Zargham and P. Gulak, "Maximum achievable efficiency in near-field coupled power-transfer systems," *IEEE Trans. Biomed. Circuits Syst.*, vol. 6, no. 3, pp. 228–245, Jun. 2012.
 [22] Y. Narusue, Y. Kawahara, and H. Morikawa, "Load optimization factors for analyzing the efficiency of wireless power transfer systems using two-port network parameters," *IEICE Electron. Exp.*, vol. 17, p. 20200093, 2020.
 [23] J. Gu, G. Zhu, L. Zhu, and X. Zhu, "A survey on dielectric elastomer actuators for soft robots," *Bioinspiration biomimetics*, vol. 12, no. 1, 2017, Art. no. 0 11003.
 [24] A. Sample, B. Waters, S. Wisdom, and J. Smith, "Enabling seamless wireless power delivery in dynamic environments," *Proc. IEEE Proc. IRE*, vol. 101, no. 6, pp. 1343–1358, 2013.
 [25] Z. Li, Y. Wang, C. C. Foo, H. Godaba, J. Zhu, and C. H. Yap, "The mechanism for large-volume fluid pumping via reversible snap-through of dielectric elastomer," *J. Appl. Phys.*, vol. 122, no. 8, 2017, Art. no. 0 84503.